RESEARCH ARTICLE

ELECTROOPTICS

Ferroelectric crystals with giant electro-optic property enabling ultracompact Q-switches

Xin Liu[1]†, Peng Tan[2,3]†, Xue Ma[4], Danyang Wang[5], Xinyu Jin[2], Yao Liu[1], Bin Xu[4], Liao Qiao[1], Chaorui Qiu[1], Bo Wang[6], Weigang Zhao[1], Chaojie Wei[7], Kexin Song[1], Haisheng Guo[1], Xudong Li[7], Sean Li[5], Xiaoyong Wei[1], Long-Qing Chen[6], Zhuo Xu[1], Fei Li[1]*, Hao Tian[2]*, Shujun Zhang[8]*

Relaxor-lead titanate ($PbTiO_3$) crystals, which exhibit extremely high piezoelectricity, are believed to possess high electro-optic (EO) coefficients. However, the optical transparency of relaxor-$PbTiO_3$ crystals is severely reduced as a result of light scattering and reflection by domain walls, limiting electro-optic applications. Through synergistic design of a ferroelectric phase, crystal orientation, and poling technique, we successfully removed all light-scattering domain walls and achieved an extremely high transmittance of 99.6% in antireflection film–coated crystals, with an ultrahigh EO coefficient r_{33} of 900 picometers per volt (pm V^{-1}), >30 times as high as that of conventionally used EO crystals. Using these crystals, we fabricated ultracompact EO Q-switches that require very low driving voltages, with superior performance to that of commercial Q-switches. Development of these materials is important for the portability and low driving voltage of EO devices.

Precise control of light propagation and intensity is critical to numerous photonic devices ranging from lasers to optical amplifiers and modulators (*1*, *2*). The rapid and efficient control of optical signals through electrical stimulus requires electro-optic (EO) materials that exhibit large changes in their refractive indices n in response to an applied electric field; e.g., the Pockels effect (*3*–*5*). The primary merits of the Pockels effect include the linear correlation between the change in refractive indices n and the applied electric field, fast responses, and a strong ability to control light, all of which are central to a wide range of photonics applications.

Ferroelectric crystals represented by $LiNbO_3$ (LN) and KD_2PO_4 (DKDP) are an important component of existing EO devices because of their availability in large size and good temperature stability (*6*, *7*). DKDP has very high optical damage thresholds suited for high-power Q-switch use (*8*). However, its hygroscopic feature requires careful protection against moisture, and thus DKDP based on EO devices require complicated fabrication processes (*9*). Further, the relatively low effective EO coefficients r_c of the LN and DKDP crystals (~21 and 24 pm V^{-1}, respectively) require the use of high voltage and/or thick material in EO devices, leading to high auxiliary cost (high voltage power supply) and difficulty in miniaturization (*10*). This issue has become a key obstacle for improving device performance. Therefore, the discovery and employment of alternative materials possessing larger Pockels effects to minimize the driving voltage and size of EO devices is highly desirable.

Many perovskite ferroelectric single crystals with substantial Pockels coefficients on the order of 10^2 pm V^{-1} —such as $BaTiO_3$, $KNbO_3$, and $Pb(Mg_{1/3}Nb_{2/3})O_3$–$PbTiO_3$ (PMN-PT)—have been developed to address the issues (*11*–*13*). Despite the promising EO properties, optical clarity of perovskite ferroelectrics is a long-standing challenge that greatly hinders practical applications of these crystals. The presence of naturally occurring ferroelectric domain walls in the crystals drastically limits their optical transparency as a result of light scattering and reflection at domain walls arising from the difference in refractive indices of the adjacent domains with different orientations, rendering high optical loss or even opacity in the visible-to-near-infrared spectrum. In the past few decades, considerable efforts have been made to eliminate the light-scattering domain walls in these ferroelectrics, but with very limited success (*13*–*21*). For example, poling a ferroelectric crystal along its polar direction can achieve a single-domain state without domain walls. However, the EO coefficients of single-domain crystals are much smaller than those of the crystals poled along a specific nonpolar direction, i.e., a domain-engineered state (*13*). More recent efforts to manipulate the domain structures of PMN-PT single crystals through ac electric field poling has demonstrated a viable approach to largely reduce the light-scattering domain walls in domain-engineered PMN-PT crystals (*19*). Although the optical transparency along the poling direction is greatly improved and a relatively high EO coefficient (r_{33}~220 pm V^{-1}) can be achieved on the basis of this method, the crystal remains opaque along the other orthogonal directions (fig. S1). Thus, designing EO devices on the basis of PMN-PT crystals remains difficult because of the challenges in obtaining high optical clarity in conjunction with giant EO performance in the crystals.

We developed a specific high-temperature poling process for [011]-oriented $Pb(In_{1/2}Nb_{1/2})O_3$-$Pb(Mg_{1/3}Nb_{2/3})O_3$-$PbTiO_3$ (PIN-PMN-PT) relaxor ferroelectric crystals to boost transparency in mutually orthogonal directions through removal of undesired domain walls, and to achieve high EO coefficients through the facilitated electric field–induced polarization rotation. This highly transparent PIN-PMN-PT crystal exhibits an ultrahigh EO coefficient r_{33} in the range of 900 to 2800 pm V^{-1}, with a temperature range of 20° to 100°C and a frequency range of 10 to 10^4 Hz. We used such poled PIN-PMN-PT crystals to construct an ultracompact free-space EO Q-switch and demonstrated its feasibility and effectiveness in miniaturization and driving voltage reduction as compared with the state-of-the-art EO devices.

Selection of relaxor ferroelectric crystals

We selected the rhombohedral 0.21PIN-(0.79 – x)PMN-xPT (x = 0.28, 0.30, 0.32) crystals as example materials, as they possess comparable room-temperature electrical properties (e.g., dielectric and piezoelectric properties) but have much improved temperature and electric field stabilities compared with those of the actively studied relaxor ferroelectric crystals PMN-PT (*22*). To achieve high transparency along both the poling and transverse directions in PIN-PMN-PT crystals, we selected the rhombohedral PIN-PMN-PT crystal with three principal axes along the crystallographic [0$\bar{1}$1], [100], and [011] directions. We show phase-field simulated domain structures for the rhombohedral crystal poled along the [011]direction (Fig. 1, A to C). Only two domain variants with polarization along the [111] and [$\bar{1}$11] directions remain in the crystal, forming 71° domain walls. The horizontal 71° domain walls are curved in the view of the (100)plane, whereas they are almost perfectly straight (parallel along the [100] direction) in the view of the (0$\bar{1}$1)

[1]Electronic Materials Research Lab, Key Lab of Education Ministry and State Key Laboratory for Mechanical Behavior of Materials, School of Electronic Science and Engineering, Xi'an Jiaotong University, Xi'an, 710049, China. [2]School of Physics, Harbin Institute of Technology, Harbin 150001, China. [3]Center of Ultra-Precision Optoelectronic Instrument Engineering, Key Laboratory of Micro-Systems and Micro-Structures Manufacturing of Ministry of Education, Harbin Institute of Technology, Harbin 150001, China. [4]School of Physical Science and Technology, Soochow University, Suzhou, Jiangsu 215006, China. [5]School of Materials Science and Engineering, The University of New South Wales, Sydney, NSW 2052, Australia. [6]Department of Materials Science and Engineering, Materials Research Institute, The Pennsylvania State University, University Park, PA 16802, USA. [7]National Key Laboratory of Science and Technology on Tunable Laser, Harbin Institute of Technology, Harbin 150001, China. [8]Institute for Superconducting and Electronic Materials, Australian Institute for Innovative Materials, University of Wollongong, Wollongong, NSW 2500, Australia.
*Corresponding author. Email: ful5@xjtu.edu.cn (F.L.); tianhao@hit.edu.cn (H.T.); shujun@uow.edu.au (S.Z.)
†These authors contributed equally to this work.

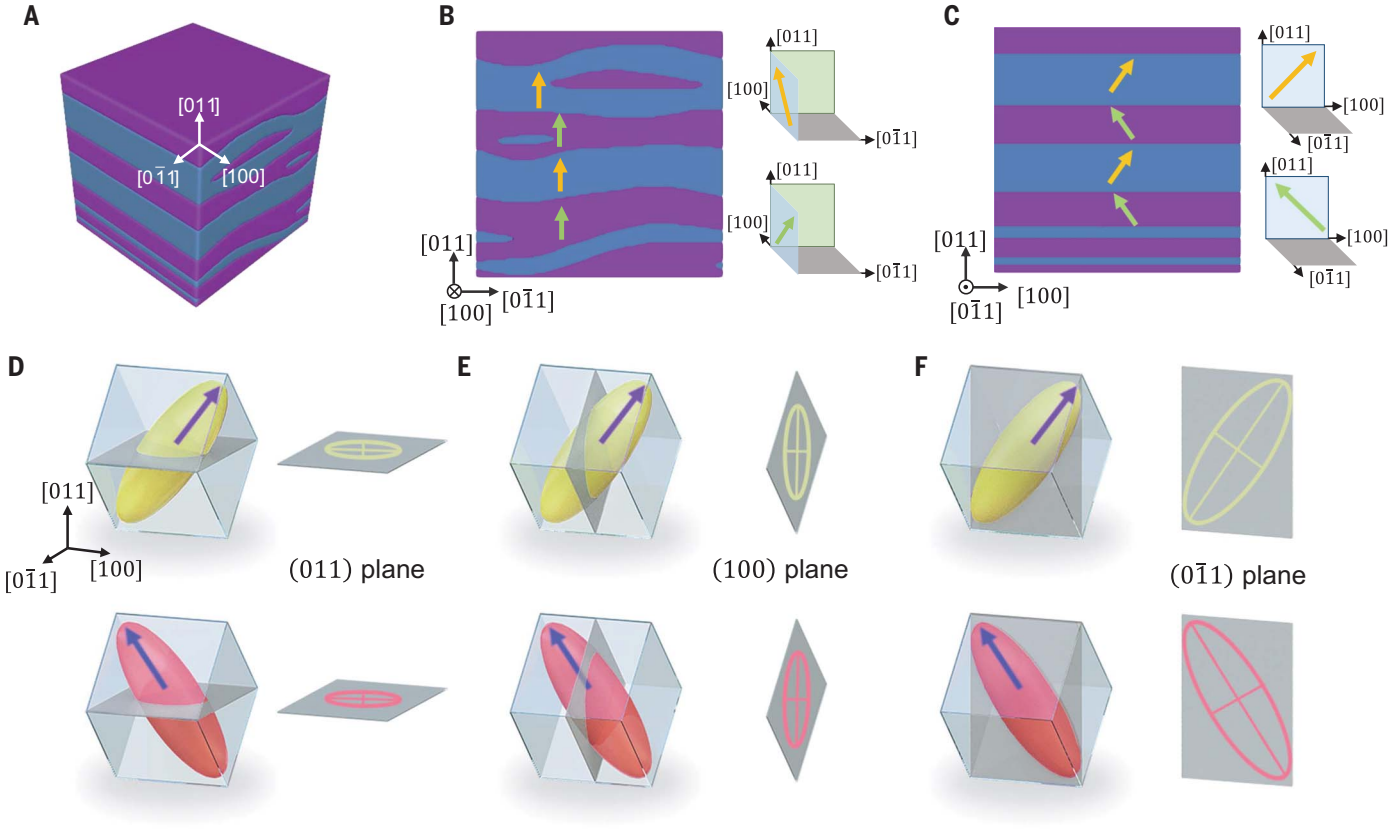

Fig. 1. Simulated domain patterns and optical indicatrix of each domain in a [011]-poled rhombohedral PIN-PMN-PT crystal. (**A**) Domain structures in the [011]-poled PIN-PMN-PT crystal under stress-free conditions on the basis of phase field simulations. (**B**) Domain pattern on a (100)plane. (**C**) Domain pattern on a (0$\bar{1}$1) plane. Purple and navy colors represent different ferroelectric domains with polarization vectors along the [$\bar{1}$11] (green) and [111](yellow) directions, respectively. (**D** to **F**) Schematic diagrams of optical indicatrix for both domains projected on the (011), (100), and (0$\bar{1}$1) planes, respectively. As shown here, the principal axes of the refractive indicatrix in both the [111] and [$\bar{1}$11] domains projected on the (011) or (100) planes are the same, leading to suppressed light scattering and/or reflection along the [011] and [100] axes. By contrast, projections of the principal axis of the optical indicatrix in neighboring domains on the (0$\bar{1}$1) plane form an angle of 71°. The alternation of the refractive indices n_o and n_e causes scattering and/or reflection of light when light travels along the [0$\bar{1}$1] direction.

plane (Fig. 1, B and C). This feature is due to the fact that the rotation of the 71° domain wall plane around the [0$\bar{1}$1] direction substantially increases the electrical and elastic energies compared with that rotates around the [100] direction (fig. S2). Therefore, the fluctuation of the 71° domain walls in the (0$\bar{1}$1) plane is prohibited, whereas small fluctuation is allowed in the (100) plane.

Considering the characteristics of the refractive indices in the [011]-poled rhombohedral crystal, high optical transparency is expected along the [011] or [100] direction. Projections of the principal axes of the optical indicatrix for the [111] and [$\bar{1}$11] domains on the (011) plane are identical (Fig. 1D). The same scenario holds true for the projections on the (100) plane (Fig. 1E). This observation suggests that the refractive indices remain unchanged as light goes across the 71° domain walls for the [011] or [100] crystallographic direction, resulting in the suppression of light scattering and/or reflection. By contrast, the optical transparency is low along the [0$\bar{1}$1] direction, considering that projection of the principal axes of the optical indicatrix on the (0$\bar{1}$1) plane is different for the [111] and [$\bar{1}$11] domains (Fig. 1F).

In addition to optical transparency, the [011]-poled rhombohedral crystals are also expected to possess high electro-optic coefficients. As the electric field is applied along the [011] direction—which is not parallel to the polar directions of the two domains, i.e., [111] or [$\bar{1}$11]—the polarization rotation in the domains can be induced (*22*, *23*). One of the most important features of relaxor ferroelectric crystals such as PIN-PMN-PT is the ease of polarization rotation under an external electric field along the nonpolar direction, which is associated with the flattened free energy landscape near the morphotropic phase boundary and the presence of nanoscale local structure heterogeneity (*23*, *24*). Consequently, the rotation of optical indicatrix in relaxor ferroelectric crystals may occur more readily in contrast to the classical ferroelectrics when subjected to external stimuli such as an electric field, leading to larger electro-optic activity in relaxor ferroelectrics.

Poling of the PIN-PMN-PT crystal

Ideally, only two kinds of ferroelectric domains (i.e., the domains with polarization along the [111] and [$\bar{1}$11] directions) should be present in the [011]-poled rhombohedral PIN-PMN-PT crystal (*25*) (Fig. 1A). In reality, however, completely removing the four electric-field–unfavored variants of ferroelectric domains (i.e., the [11$\bar{1}$], [$\bar{1}$1$\bar{1}$], [$\bar{1}\bar{1}$1], and [1$\bar{1}$1] domains) is difficult because of the clamping effect from the sample surface (*26*), which severely scatters the light. The results of the phase field simulation under clamping conditions (Fig. 2A and fig. S3) show that some domains with polarization perpendicular to the [011] axis are present to release the elastic energies during the removal of the poling electric field. We also experimentally verified the influence of the clamping effect on the final domain state (movie S1 and fig. S4). We used a polarized light microscope (PLM) to obtain images of a [011]-oriented 0.21PIN-0.47PMN-0.32PT (PIN-PMN-32PT) crystal poled with a conventional poling method, i.e., at room temperature under an electric field of twice

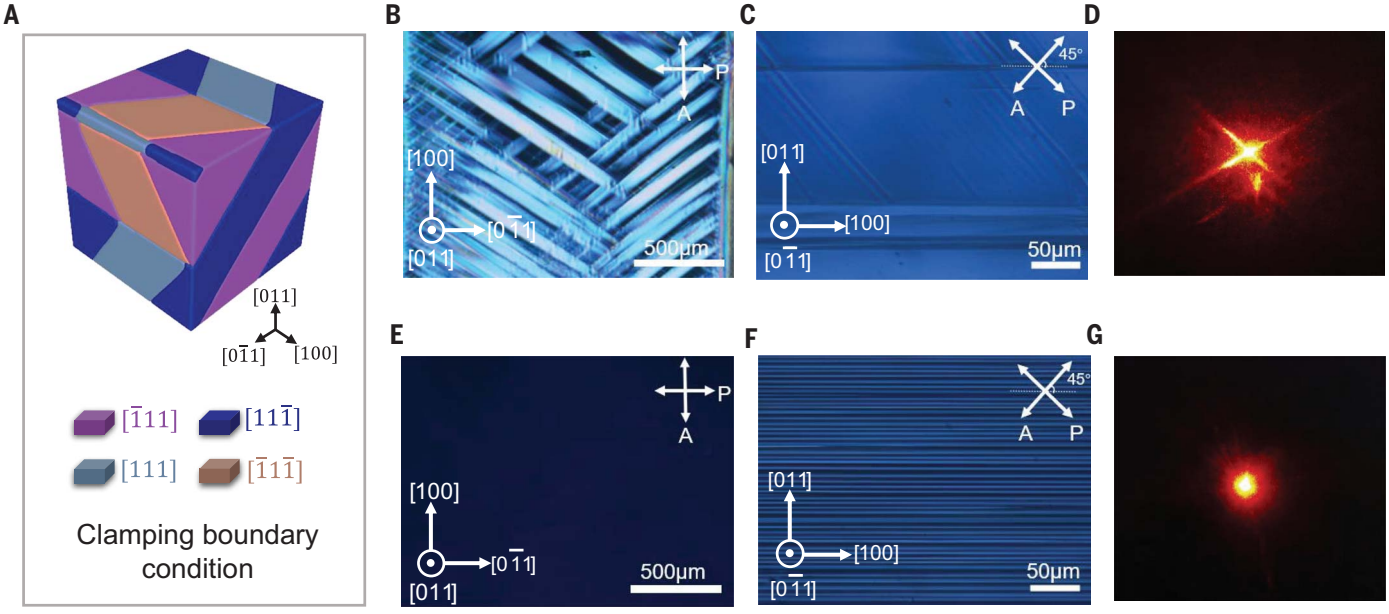

Fig. 2. Domain structures for [011]-oriented rhombohedral PIN-PMN-32PT crystals poled by conventional and high-temperature methods. (**A**) Domain structure of the [011]-poled sample under clamped conditions from phase field simulations. It should be noted that only two domains with polarization perpendicular to the [011] direction are present in Fig. 2A, which is due to the fact that the scale of phase field simulation (64 nm by 64 nm by 64 nm) is much smaller than that of a real sample. We also conducted a phase field simulation involving the other two domains (polarizations are along the $[\bar{1}1\bar{1}]$ and $[\bar{1}11]$ directions) (fig. S3). (**B** and **C**) PLM images on (011) and $(0\bar{1}1)$ surfaces of the [011]-oriented crystals poled by conventional poling method, respectively. (**D**) Output spot of a Gaussian beam which propagates along the [011] direction of the crystal poled by the conventional poling method. (**E** and **F**) PLM images on the (011) and $(0\bar{1}1)$ surfaces, respectively, of the [011]-oriented crystals poled by high-temperature poling method, respectively. The width of the laminar domains of the sample in Fig. 2F is 2.77 μm (SD ~±1.72 μm). (**G**) Output spot of a Gaussian beam that propagates along the [011] direction of the crystal poled by the high-temperature poling method.

the coercive field. (Fig. 2, B and C, and fig. S5). The PLM images taken from the (011) and $(0\bar{1}1)$ surfaces are consistent with the simulated domain structure (Fig. 2A). A number of domain walls are visible in Fig. 2B, in which the angle between the domain walls and $[0\bar{1}1]$ direction is ~35°. The domain walls presented in Fig. 2B are mainly formed by [111] or $[\bar{1}11]$ domain with one of the $[11\bar{1}]/[\bar{1}1\bar{1}]/[\bar{1}11]/[1\bar{1}1]$ ferroelectric domains whose polarization lies in the (011) plane (fig. S6). Because of the presence of these light-scattering domain walls, a 633-nm Gaussian beam with a circular cross section is strongly scattered as the beam goes through the crystal (Fig. 2D). The shape of the scattered beam spot nearly replicates the domain pattern (Fig. 2B) as a result of the diffraction from the refractive indices discontinuity at domain walls (*27*). Evidently, the light scattering will reduce the transparency and adversely affect the efficiency of EO devices.

We employed a high-temperature poling approach to reduce the clamping effect and eliminate the light-scattering domain walls. Specifically, the crystal was heated to ~105° to 115°C and was thus in the orthorhombic phase. Then, by applying an electric field of 5 kV cm^{-1}, we can achieve orthorhombic single-domain configuration. Finally, the crystal was slowly cooled to room temperature with the application of the electric field. During cooling, the orthorhombic single domain with polarization along the [011] direction only split into the rhombohedral [111] and $[\bar{1}11]$ domains. Throughout the process, other variants of rhombohedral domains were absent (movie S2 and fig. S7). By using the above poling strategy, we obtained [011]-poled PIN-PMN-PT crystals without the undesired domains (i.e., $[11\bar{1}]$, $[\bar{1}1\bar{1}]$, $[\bar{1}11]$, or $[1\bar{1}1]$; Fig. 2, E and F, and fig. S8). We observed the extinction phenomenon as the incident light is along the [011] direction with polarization along the $[0\bar{1}1]$ direction (Fig. 2E), whereas the lamellar domain configuration is observed from the $(0\bar{1}1)$ (Fig. 2F) and (100) (fig. S8) planes, which echoes the simulated domain structure under stress-free conditions (Fig. 1A). As expected, the footprint of the Gaussian beam remains as a circular spot after transmitting this crystal along the [011] axis (Fig. 2G), implying substantially enhanced light transmittance compared with that the crystal poled at room temperature. The PIN-PMN-PT crystals used for the discussion of EO properties as well as device design are poled by the high-temperature poling technique.

Transparency and electro-optic properties of the [011]-poled PIN-PMN-PT crystal

We photographed [011]-poled PIN-PMN-PT crystals (Fig. 3A). The poled crystals are highly transparent when viewed from both the [100] and [011] directions. The light transmittance along both directions of the poled sample is ~70% in the wavelength range of 550 to 2500 nm, which is very close to the theoretical limit if only surface reflection is considered (Fig. 3B). Additionally, the [011]-poled PIN-PMN-PT crystal exhibits high transparency in the intermediate infrared band, i.e., 2500 to 5500 nm (Fig. 3C), except for a small absorption peak around the wavelength of 2840 nm resulting from the stretching vibrations of OH^- ions, which was observed in many perovskites such as $SrTiO_3$, $BaTiO_3$, $LiNbO_3$, and $KTaO_3$ (*28*–*30*). We found the optical absorption to monotonically decrease with increasing wavelength (Fig. 3D). As a result of the improved poling technique, the optical transmittance of the present PIN-PMN-PT crystal is considerably higher than that of previously reported relaxor ferroelectric crystals (*14*, *31*–*33*). The transmittance can be further improved through the coating of antireflective film on the transparent surface, e.g., the (100) surface (blue curve in Fig. 3B). In particular, at a wavelength of 1064 nm the optical transmittance is 99.6%, in which the optical absorption of the crystal and surface reflection loss are 0.16 and 0.24%, respectively.

We measured the Pockels coefficients r_{13} and r_{33} with the Mach-Zehnder interferometer (fig. S9A), whereas the effective EO coefficient

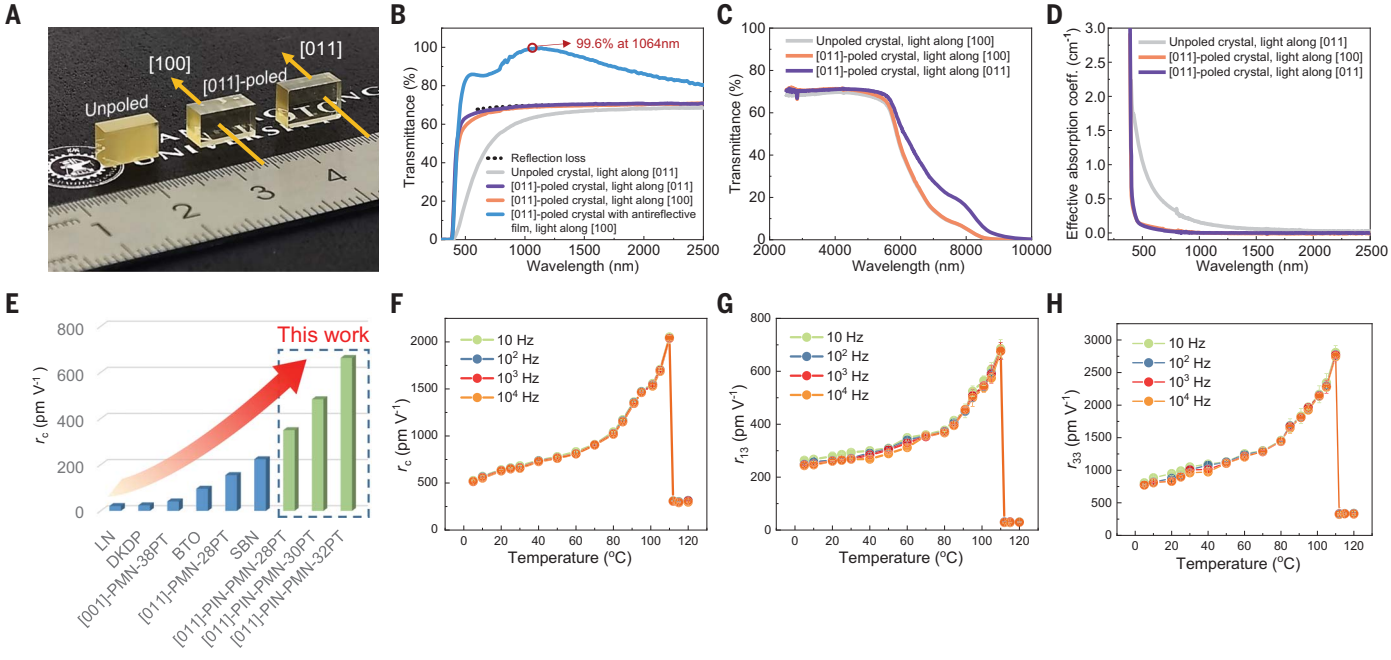

Fig. 3. Transparency and electro-optic properties of PIN-PMN-PT crystals poled along the [011] direction by the high-temperature poling method. Photograph of poled PIN-PMN-PT single crystals with the major faces of (100) and (011), respectively. An unpoled crystal is also given for comparison. The sample size in (**A**) is 8 mm by 3.5 mm by 3 mm. (**B**) Optical transmittance spectra of PIN-PMN-PT samples before and after poling and with antireflective coating (sample thickness is 1.5 mm for optical transmittance measurements). (**C**) Optical transmission spectra of [011]-poled PIN-PMN-PT samples within the wavelength of 2500 to 10,000 nm. (**D**) Effective absorption coefficient of the [011]-poled and unpoled PIN-PMN-PT crystals. (**E**) Comparison of EO coefficient r_c (at room temperature) between [011]-poled PIN-PMN-PT crystals and state-of-the-art EO crystals. (**F** to **H**) Frequency and temperature dependences of r_c, r_{13}, and r_{33}, respectively, for the [011]-poled PIN-PMN-32PT crystal. The error bars indicated the standard errors measured from five points of a sample. It should be noted that EO coefficients can be greatly enhanced as the test frequency approaching the piezoelectric resonance frequency of the sample (fig. S11). This phenomenon is related to the greatly enlarged piezoelectric displacement at the resonance frequency.

r_c was measured with the Senarmont compensator method (fig. S9B) (*34*). We chose a 633-nm He-Ne laser as the light source for the measurement of EO properties. For the rhombohedral PIN-PMN-PT crystals, we found that the EO coefficient r_c increases with increasing PT content, i.e., with the composition approaching the morphotropic phase boundary (MPB) (Fig. 3E). We can attribute this feature to the electric field–induced polarization rotation becoming easier as the composition approaches the MPB (*22*). We mainly focused the following discussion on the PIN-PMN-32PT crystal, which possesses the highest EO coefficient r_c among all studied compositions.

At room temperature (25°C), the r_{33}, r_{13}, and r_c coefficients of the PIN-PMN-32PT crystal were found to be 910, 260, and 670 pm V^{-1}, respectively, outperforming the actively studied EO crystals (Fig. 3E and fig. S10). It is worth noting that the contributions from the variation of the optical path length—which is induced by the converse piezoelectric effect under the applied electric field—to coefficients r_{33}, r_{13}, and r_c are 299, 296, and −4 pm V^{-1}, respectively (*34*). The coefficient r_c is ~30 times as large as that of the state-of-the-art LN and DKDP EO crystals, confirming the potential for use in compact EO devices with low driving voltage. Some other ferroelectric materials may also possess high EO coefficients (r_c > 200 pm V^{-1}), such as (Sr,Ba)Nb_2O_6 crystals (*35*), but these high values are a result of the ferroelectric phase transition temperature being close to room temperature, which greatly limits their operating temperature range. In addition, the EO coefficients of PIN-PMN-32PT crystals are much higher than that of previously reported relaxor ferroelectric crystals, including [011]-poled PMN-28PT (*21*). This is due to the following two reasons: First, the composition of PIN-PMN-32PT is closer to the MPB when compared with the reported PMN-28PT. The electric field-induced polarization rotation becomes easier as the composition approaches the MPB, leading to the higher EO property. Second, by the high-temperature poling technique, the undesired domains in PIN-PMN-32PT crystals can be completely removed without any irreversible electric field-induced phase transition. It is generally believed that the crystal with MPB compositions can be partially transformed into the orthorhombic phase by [011] electric field poling at room temperature because of the over-poling effect, leading to the greatly reduced EO property. By contrast, the applied electric field used in high-temperature poling is much lower than that for room-temperature poling, and thus the PIN-PMN-32PT crystal can fully recover to the rhombohedral phase with the desired domain structure during cooling.

To understand the origin of the giant EO coefficients in rhombohedral PIN-PMN-PT crystals, we performed density functional theory (DFT) calculations. A typical relaxor-PT composition, i.e., 0.75PMN-0.25PT (PMN-25PT), was selected for the calculation as it allows a supercell size feasible for DFT calculations (*36*, *37*); further, its electro-optic and piezoelectric properties are comparable to our studied PIN-PMN-32PT crystal. Through the approach proposed in (*38*–*41*), the intrinsic EO coefficient r_{ijk} under stress-free conditions can be expressed as

$$r_{ijk} = r_{ijk}^{\mathrm{el}} + r_{ijk}^{\mathrm{ion}} + r_{ijk}^{\mathrm{piezo}} \quad (1)$$

The first term r_{ijk}^{el} is a pure electronic part, the second term r_{ijk}^{ion} corresponds to the ionic contribution, and the last term r_{ijk}^{piezo} corresponds to the coupling of piezoelectric and elasto-optic effects. The three contributions were calculated at 0 K for the PMN-25PT crystal. According to our DFT calculations (*34*), the EO coefficients calculated at 0 K (<50 pm V^{-1}, see table S1) are much smaller than those

measured at room temperature. At a temperature far below the phase transition point, the electronic contribution is expected to be insensitive to temperature because it is related to the interaction of the applied electric field with the valence electrons, whereas the ions are confined to their equilibrium positions (*41*). For the PIN-PMN-32PT crystal, the rhombohedral-orthorhombic phase transition temperature and Curie temperature are 105° and 180°C, respectively. Thus, the high EO coefficients at room temperature are thought to be related to the ionic and piezoelectric contributions (i.e., the components r_{ijk}^{ion} and r_{ijk}^{piezo}). These are, in a reasonable approximation, proportional to the dielectric and the piezoelectric tensors, respectively (*34*). The calculated dielectric constant and piezoelectric coefficient of PMN-25PT are lower than 70 and 110 pm V^{-1}, respectively, at 0 K (tables S2 and S3), whereas the measured values are up to 3500 and 1200 pm V^{-1}, respectively, at room temperature, showing a substantial positive correlation with temperature. Therefore, it should be inferred that the components r_{ijk}^{ion} and r_{ijk}^{piezo} increase substantially with temperature as they are responsible for the high room temperature EO coefficients for the PIN-PMN-32PT crystals.

To validate this inference, we measured the EO coefficients of the PIN-PMN-32PT crystal as a function of temperature (Fig. 3, F to H). As the temperature increases from 5 to 60°C, we found that the EO coefficients increase by ~30 to 50%, as they are similar to the temperature-induced changes of the dielectric and piezoelectric coefficients (*22*), revealing that dielectric- and piezoelectric-related contributions play a key role in EO coefficients. The EO coefficients are substantially reduced at a temperature above the rhombohedral-orthorhombic phase transition temperature $T_{r\text{-}o}$ (~105°C), because of both the low piezoelectricity in the orthorhombic phase along the [011] direction and the depoling effect during the phase transition.

In contrast to the strong temperature dependence, the EO coefficients of the PIN-PMN-32PT crystal exhibit excellent stability with respect to frequency. The r_{33}, r_{13}, and r_c coefficients exhibit minor variation below 5% within the frequency range of 10 to 10^4 Hz (Fig. 3, F to H). This feature is vital for EO devices that operate over a broad frequency range, e.g., electro-optic modulators used in the field of broadband radar.

Electro-optic Q-switch made of PIN-PMN-PT crystals

To demonstrate the competitive advantages of our PIN-PMN-PT crystals in practical applications, we constructed and characterized electro-optic Q-switches. Because of the large EO properties and relatively high laser damage threshold (~500 MW cm^{-2}) (*42*), PIN-PMN-PT crystals are promising candidates for Q-switching applications that require ultracompact size and greatly reduced driving voltage.

For benchmark purposes, we also explored key properties of commercial DKDP- and LN-based Q-switches when housed in the same laser cavity for the characterization of the PIN-PMN-32PT Q-switch. We show the commercial DKDP- and LN-based Q-switches and a compact low-voltage Q-switch made of the PIN-PMN-32PT crystal with size 5 mm by 5 mm by 1.5 mm (Fig. 4A). The dimensions of the PIN-PMN-32PT Q-switch are ϕ 12 mm by 3.4 mm, which are considerably smaller than those of the DKDP Q-switch (ϕ 15 mm by 18 mm) and LN Q-switch (ϕ 22 mm by 22 mm); this small size is attributable to its ultrahigh effective EO coefficient, r_c (Fig. 3E). Theoretically, reducing the Q-switch optical travel length is accompanied by an increase in operating voltage, according to Eq. 2

$$V_{\pi/2} = \frac{\lambda d}{2n^3 r_c l} \tag{2}$$

in which $V_{\pi/2}$ is the quarter-wave voltage (i.e., the operating voltage), λ is the wavelength, n is the refractive index, r_c is the effective EO coefficient, l is the length of the crystal along the optical travel direction, and d is the distance between two electrodes of the EO crystal. Because of the ultrahigh EO coefficients, the operating voltage of the studied PIN-PMN-32PT crystal is only 0.2 kV, suggesting 16- and 6.5-fold reductions when compared with that of DKDP and LN, respectively.

We illustrated the laser cavity setup for experimentally characterizing the performance of the PIN-PMN-32PT Q-switch (Fig. 4B). This cavity accommodates a rear mirror, a polarizing beam splitter, an α-cut Nd:YVO_4 acting as the laser host crystal, the Q-switch, a quarter-wave plate, an eighth-wave plate, and an output mirror. The total length of the laser cavity is 65 mm. To ensure that the Q-switch is in high-loss mode under the hold-off state, the position of the eighth-wave plate was carefully adjusted to compensate for the phase retardation induced by the initial birefringence of the PIN-PMN-32PT crystal, leading to zero laser output power. A pulsed laser with a wavelength of 1064 nm is generated at the output end of the cavity through application of a control signal on the PIN-PMN-32PT Q-switch, i.e., pulsed $V_{\pi/2}$ voltage with a repetition rate of 10 Hz to 2 kHz.

We show a single output pulse generated by the PIN-PMN-32PT Q-switch and compared it with commercial DKDP and LN Q-switches at a repetition rate of 1 kHz and pump energy of 3.7 mJ (Fig. 4C). The pulse width of the PIN-PMN-32PT Q-switch is on the order of 1.8 ns—a slight improvement compared with those of commercial Q-switches. The PIN-PMN-32PT Q-switch can produce a more symmetric pulse (Fig. 4C) with a consistently narrower pulse width over a relatively wide repetition rate span (10 Hz to 2 kHz) and pump energy (~2.3 to 3.7 mJ) compared with those of their DKDP- and LN-based counterparts (Fig. 4, D and E). In general, the width of a Q-switched pulse is positively correlated with the intracavity propagation time of the laser beam (*43*). The compact size of the studied PIN-PMN-32PT crystal excessively minimizes the additional optical path length induced by the insertion of the Q-switch (i.e., a product of the geometric length of the crystal along the laser travel direction and the refractive indices of the EO crystal). Consequently, the intracavity propagation time of the PIN-PMN-32PT Q-switched laser is shorter and more strongly favors the narrowing of the output pulse width.

The PIN-PMN-32PT Q-switched laser exhibits a satisfactory output pulse energy and optical-to-optical efficiency (~7.7%) at a repetition rate of 1 kHz (Fig. 4F), both of which are highly comparable to those of the laser pulses generated by the commercial DKDP- and LN-based Q-switches, with efficiency on the order of 7.9 and 8.0%, respectively.

Peak power, represented by the pulse energy and pulse width, is another key parameter for understanding the performance of a Q-switch. The maximum peak power of the pulse produced by the studied PIN-PMN-32PT Q-switch was calculated to be 154 kW at input pumping energy of 3.7 mJ, which is nearly identical to that of the DKDP- and LN-based Q-switched laser (Fig. 4G and table S4). This substantial peak power is primarily ascribed to the shorter pulse width, which effectively offsets the minor deficiency in the output pulse energy. This result provides further evidence that the studied PIN-PMN-32PT crystals are of extremely high quality in terms of optical transparency and homogeneity and thus meet the standards of a commercial product.

The pulse-to-pulse energy stability of the pulse train is also an important feature for evaluating Q-switch performance. We recorded the energy profile of 100 sequential output pulses produced by the PIN-PMN-32PT Q-switch at a pump energy of 3.7 mJ and a repetition rate of 1 kHz (Fig. 4H). The variation coefficient of the laser output energy over the pulse train is estimated to be 2.7%, demonstrating an ultralow output energy jitter on par with that of the commercial DKDP and LN Q-switches (Fig. 4I and fig. S12).

Through ferroelectric phase, crystal orientation, and poling process designs, we successfully boosted the transparency of PIN-PMN-PT crystals (99.6% at a wavelength of 1064 nm) and achieved very high EO coefficients (r_{33} and r_c of 900 and 670 pm V^{-1}, respectively). Because the PIN-PMN-PT crystals have desirable electro-optic properties, we used them for

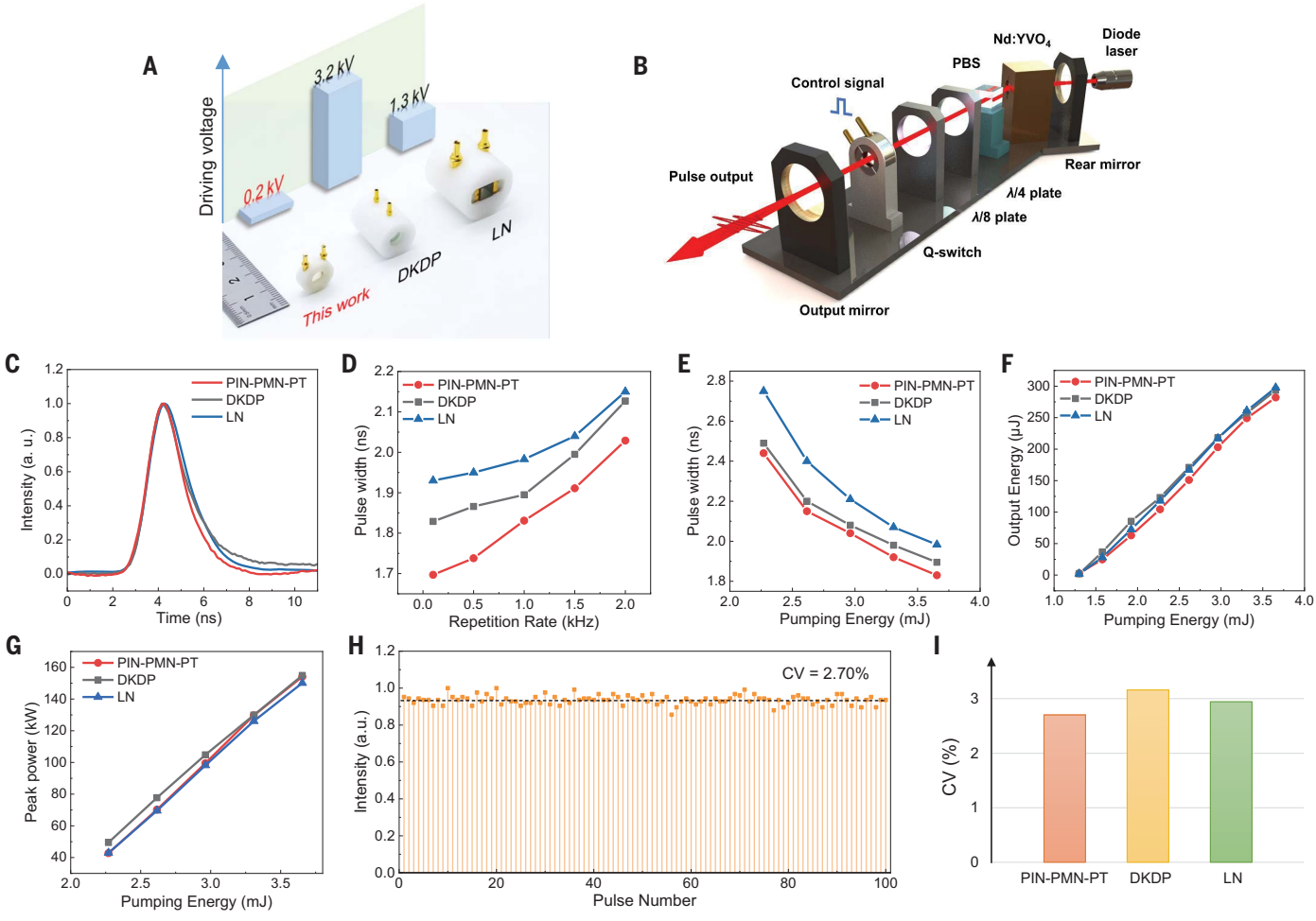

Fig. 4. Key performances of the Q-switch fabricated by the transparent PIN-PMN-32PT crystal. (**A**) EO Q-switch based on different crystals, in which operating voltages $V_{\pi/2}$ (at 1064 nm) are given as well. For PIN-PMN-32PT and LN-based Q-switches, the light travel direction and applied electric field direction are perpendicular, whereas for the DKDP-based Q-switch, the light and electric field are along the same direction. (**B**) Schematic of Nd:YVO_4 laser Q-switched by PIN-PMN-32PT in the pulse-on cavity at λ = 1064 nm. (**C**) Single pulse profile of the oscillator at 1 kHz and 3.7 mJ. (**D**) Pulse width as function of repetition rate (pumping energy of 3.7 mJ). (**E**) Pulse width as a function of pumping energy (repetition rate of 1 kHz). (**F**) Output pulse energy at 1 kHz as a function of pumping energy. (**G**) Peak power as a function of pumping energy. (**H**) Recorded output pulse train consisting of 100 sequential pulses at 1 kHz, showing an ultralow energy jitter of PIN-PMN-PT-based Q-switch (CV, ratio of standard deviation to the mean value). (**I**) The CV of PIN-PMN-PT, DKDP and LN crystals, measured at 1 kHz.

the design of a free-space Q-switch. Compared with the commercial LN and DKDP-based Q-switches, the volume of the PIN-PMN-32PT-based Q-switch is substantially reduced by more than one order of magnitude, with the operating voltage reduced to 200 V from a starting point of 1300 to 3200 V. Given the fact that the Q-switch is a key component of pulsed lasers, the miniaturization and low driving voltage of the Q-switches will considerably reduce the size, weight, and power consumption of pulsed lasers while also mitigating issues relating to electromagnetic interference induced by high-voltage pulses. This development will benefit numerous applications, such as ultracompact and low-power–consumption laser radars, enable sensing functions in navigation with small-scale robots and intelligent recognition in autonomous driving, and allow for improved precision in medical and scientific equipment requiring high stability and reliability.

REFERENCES AND NOTES

1. M. Zhang *et al.*, *Nature* **568**, 373–377 (2019).
2. G. T. Reed, G. Mashanovich, F. Y. Gardes, D. J. Thomson, *Nat. Photonics* **4**, 518–526 (2010).
3. J. D. Bull, N. A. Jaeger, H. Kato, M. Fairburn, A. Reid, P. Ghanipour, "40-GHz electro-optic polarization modulator for fiber optic communications systems" in *Proc. SPIE 5577, Photonics North 2004: Optical Components and Devices* (Society of Photo-Optical Instrumentation Engineers, 2004), pp. 133–143.
4. C. Wang *et al.*, *Nature* **562**, 101–104 (2018).
5. L. R. Dalton, P. A. Sullivan, D. H. Bale, *Chem. Rev.* **110**, 25–55 (2010).
6. E. L. Wooten *et al.*, *IEEE J. Sel. Top. Quantum Electron.* **6**, 69–82 (2000).
7. H. Nakano, K. Kanz, C. A. Ebbers, "A thermally compensated, deuterated KDP Q-switch for high average power lasers" in *Summaries of Papers Presented at the Lasers and Electro-Optics. CLEO '02. Technical Diges. IEEE*, (2002) pp. 179–180.
8. G. Li *et al.*, *J. Cryst. Growth* **274**, 555–562 (2005).
9. B. A. Fuchs, P. P. Hed, P. C. Baker, *Appl. Opt.* **25**, 1733–1735 (1986).
10. M. Aillerie, N. Théofanous, M. D. Fontana, *Appl. Phys. B* **70**, 317–334 (2000).
11. M. Zgonik *et al.*, *Phys. Rev. B Condens. Matter* **50**, 5941–5949 (1994).
12. M. Zgonik, R. Schlesser, I. Biaggio, P. Günter, *Ferroelectrics* **158**, 217–222 (1994).
13. X. Wan *et al.*, *Appl. Phys. Lett.* **85**, 5233–5235 (2004).
14. X. Wan, H. Luo, J. Wang, H. L. W. Chan, C. L. Choy, *Solid State Commun.* **129**, 401–405 (2004).
15. Y. Zhao *et al.*, *Ferroelectrics* **542**, 112–119 (2019).
16. Y. Zhao *et al.*, *J. Appl. Phys.* **123**, 084104 (2018).
17. D.-Y. Jeong, Y. Lu, V. Sharma, Q. Zhang, H.-S. Luo, *Jpn. J. Appl. Phys.* **42**, 4387–4389 (2003).
18. Q. Hu *et al.*, *Appl. Phys. Lett.* **115**, 222901 (2019).
19. C. Qiu *et al.*, *Nature* **577**, 350–354 (2020).
20. F. Li, L. Wang, L. Jin, Z. Xu, S. Zhang, *Cryst. Eng. Comm.* **16**, 2892–2897 (2014).
21. C. Deng *et al.*, *Adv. Mater.* **33**, e2103013 (2021).
22. S. Zhang, F. Li, *J. Appl. Phys.* **111**, 031301 (2012).
23. H. Fu, R. E. Cohen, *Nature* **403**, 281–283 (2000).
24. F. Li *et al.*, *Nat. Commun.* **7**, 13807 (2016).

25. S. Zhang *et al*., *Prog. Mater. Sci.* **68**, 1–66 (2015).
26. Z. Chen *et al*., Giant tuning of ferroelectricity in single crystals by thickness engineering. *Sci. Adv.* **6**, eabc7156 (2020).
27. M. Müller, E. Soergel, M. C. Wengler, K. Buse, *Appl. Phys. B* **78**, 367–370 (2004).
28. F. G. Wakim, *J. Chem. Phys.* **49**, 3738–3739 (1968).
29. A. Jovanović, M. Wöhlecke, S. Kapphan, A. Maillard, G. Godefroy, *J. Phys. Chem. Solids* **50**, 623–627 (1989).
30. L. Kovács, M. Wohlecke, A. Jovanović, K. Polgár, S. Kapphan, *J. Phys. Chem. Solids* **52**, 797–803 (1991).
31. C. He *et al*., *J. Appl. Phys.* **110**, 083513 (2011).
32. F. Wu *et al*., *J. Mater. Sci.* **47**, 2818–2822 (2012).
33. E. Sun *et al*., *J. Appl. Phys.* **107**, 113532 (2010).
34. Materials and methods are available as supplementary materials.
35. S. Ducharme, J. Feinberg, R. Neurgaonkar, *IEEE J. Quantum Electron.* **23**, 2116–2121 (1987).
36. H. Takenaka, I. Grinberg, S. Liu, A. M. Rappe, *Nature* **546**, 391–395 (2017).
37. F. Li *et al*., *Science* **364**, 264–268 (2019).
38. M. Veithen, X. Gonze, Ph. Ghosez, *Phys. Rev. B Condens. Matter Mater. Phys.* **71**, 125107 (2005).
39. A. K. Hamze, A. A. Demkov, *Phys. Rev. Mater.* **2**, 115202 (2018).
40. A. K. Hamze, M. Reynaud, J. Geler-Kremer, A. A. Demkov, *Npj Comput. Mater.* **6**, 130 (2020).
41. M. Veithen, Ph. Ghosez, *Phys. Rev.* **71**, 132101 (2005).
42. W. Zhao *et al*., *Ceram. Inter.* **42**, 11909–11914 (2022).
43. W. Koechner, *Solid-State Laser Engineering*, vol. 1 (Springer, 1988).

ACKNOWLEDGMENTS

Funding: F.L., Z.X., and X.Y.W. acknowledge the support of the National Natural Science Foundation of China (grants 51922083, 51831010, and 51761145024), the development programme of Shaanxi province (grants 2019ZDLGY04-09), the National Key R&D Program of China (grant 2021YFE0115000), and the 111 Project (B14040). H.T. acknowledge the support of the National Natural Science Foundation of China (grants 12074092 and 12004085) and the fellowship of China National Postdoctoral Program for Innovative Talents (grant BX20200111). B.X. acknowledges financial support from the National Natural Science Foundation of China (grant 12074277) and the Natural Science Foundation of Jiangsu Province (BK20201404). D.W. acknowledges the support of the Australian Research Council (FT180100541). B.W. and L.Q.C. acknowledge the support of the US National Science Foundation under grant DMR-1744213 and Materials Research Science and Engineering Center (MRSEC) grant DMR-1420620. **Author contributions:** The work was conceived and designed by S.Z., H.T., and F.L.; X.L. prepared the samples, with assistance from C.Q. and L.Q.; X.L. and P.T. performed the optical experiments, with assistance from W.Z.; P.T. and X.J. fabricated the device and characterized the performances, with assistance from C.W. and X.L.; K.S. and H.G. grew the crystals; F.L. and Z.X. supervised crystal growth; F.L., X.W., and H.T. supervised the optical experiments; H.T. supervised device fabrication and characterization; X.M. and B.X. performed the DFT calculation; Y.L. and B.W. performed the phase field simulations with the supervision of F.L. and L.Q.C.; F.L. and X.L. drafted the manuscript; S.Z., D.W., S.L., and L.Q.C. revised the manuscript, and all authors discussed the results. **Competing interests:** The authors declare that they have no competing interests. **Data and materials availability:** All relevant data are available in the main text or the supplementary materials.

SUPPLEMENTARY MATERIALS

science.org/doi/10.1126/science.abn7711
Materials and Methods
Supplementary Text
Figs. S1 to S12
Tables S1 to S7
References (*44*–*63*)
Movies S1 and S2

19 December 2021; accepted 23 March 2022
10.1126/science.abn7711

Science

Ferroelectric crystals with giant electro-optic property enabling ultracompact Q-switches

Xin LiuPeng TanXue MaDanyang WangXinyu JinYao LiuBin XuLiao QiaoChaorui QiuBo WangWeigang ZhaoChaojie WeiKexin SongHaisheng GuoXudong LiSean LiXiaoyong WeiLong-Qing ChenZhuo XuFei LiHao TianShujun Zhang

Science, 376 (6591), • DOI: 10.1126/science.abn7711

Breaking down the domain walls

Ferroelectric materials should make for decent optical components because of the change in refractive index with electric field. However, many of the best ferroelectrics have domain walls that scatter light and are not useful for optics applications. Liu *et al*. used a high-temperature poling method to remove the light-scattering domain walls in a lead ceramic ferroelectric. The material has a very high electro-optic coefficient and requires a very low driving voltage. This strategy may be useful for other materials and may help in the development of better optical devices. —BG

Science (ISSN) is published by the American Association for the Advancement of Science. 1200 New York Avenue NW, Washington, DC 20005. The title *Science* is a registered trademark of AAAS.